ELSEVIER

Journal of Chromatography A, 822 (1998) 233–251

JOURNAL OF CHROMATOGRAPHY A

Prediction of comprehensive two-dimensional gas chromatographic separations
A theoretical and practical exercise

J. Beens[a,*], R. Tijssen[a], J. Blomberg[b]

[a]*Laboratory for Analytical Chemistry, University of Amsterdam, Nieuwe Achtergracht 166, 1018 WV Amsterdam, The Netherlands*
[b]*Shell Research and Technology Centre Amsterdam, Badhuisweg 3, 1031 CM Amsterdam, The Netherlands*

Received 15 June 1998; received in revised form 4 August 1998; accepted 4 August 1998

Abstract

Two-dimensional gas chromatography offers an unsurpassed and ordered separation combined with a very high peak capacity. Especially when applied to the separation and quantitative characterisation of complex mixtures it constitutes a leap forward with respect to state-of-the-art capillary GC. This is realised by the two orthogonal separations to which an entire sample is subjected. However, the selection of the proper combination of stationary phases and the temperature program is rather complicated and time consuming. A model is developed to predict which combination of columns is the most appropriate for a specified separation problem. The model is based on calculating retention times and peak widths of the compounds to be separated, on both columns, thus predicting the eventual chromatogram. It starts from estimating the retention factors (k) of the compounds at their elution temperatures. This is performed with the help of the (calculated) vapour pressures and the enthalpic contribution to the activity coefficient as obtained from the Kováts retention indices. Some examples illustrate the usefulness of the model.

Keywords: Two-dimensional gas chromatography; Peak capacity; Retention indices

1. Introduction

Modern capillary columns offer high peak capacities. A standard sized ''normal-bore'' column (0.25 mm I.D., 30 m length) has a peak capacity of the order of 1000. With the introduction of ''narrow-bore'' columns (50–100 μm I.D.) the number of theoretical plates per meter has been significantly increased, but so has the pressure drop across the column. With this type of column the separation time can be decreased drastically, but due to pressure limitations the peak capacity remains of the same order of magnitude. None of these columns however, comes close to separating all the individual constituents of complex samples. A typical petrochemical sample in the middle distillate range (150–400°C) may contain several hundreds of thousands of compounds. Multidimensional chromatography, such as contemporary (heart-cut) GC–GC [1,2] or LC–GC [3,4] are able to characterise (parts) of these complex samples, but only at the expense of very long separation times and complex instrumentation.

With the introduction of comprehensive two-dimensional (2D) gas chromatography (GC×GC) [5–7] a technique has become available, especially suited for separating and identifying components of

*Corresponding author.

0021-9673/98/$ – see front matter
PII: S0021-9673(98)00649-9

complex samples. In GC×GC two independent GC separations are applied to an entire sample. The sample is first separated on a high-resolution capillary GC column under programmed-temperature conditions. The effluent of this column is then focused in very small fractions and in very short time intervals reinjected by means of a thermal modulator onto a second column. This second column is shorter and narrower to allow for very rapid separations. The separation in this fast column must be finished before the next reinjected fraction will start to elute. The speed of the second column is so high that it is effectively operated under isothermal conditions.

The resulting chromatogram is in fact a surface in a three-dimensional (3D)-space, of which two axes represent the retention times of solutes of the first and the second column respectively, while the third axis represents the detector response, which corresponds to the peak heights. An example of a 3D-representation of a (part of a) separation of a petrochemical oil (cracked product) is presented in Fig. 1.

When displaying the chromatogram as a contour plot, within the 2D-plane of the two retention time axes, compounds are ordered according to their chemical or molecular functionality, structure or shape, which makes identification relatively easy and reliable. GC×GC offers tremendously high peak capacities; the total peak capacity being approximately equal to the arithmetic product of the peak capacities of both columns [5]. By selecting a proper combination of phases, unsurpassed separations can thus be established.

In GC×GC two types of separations can be

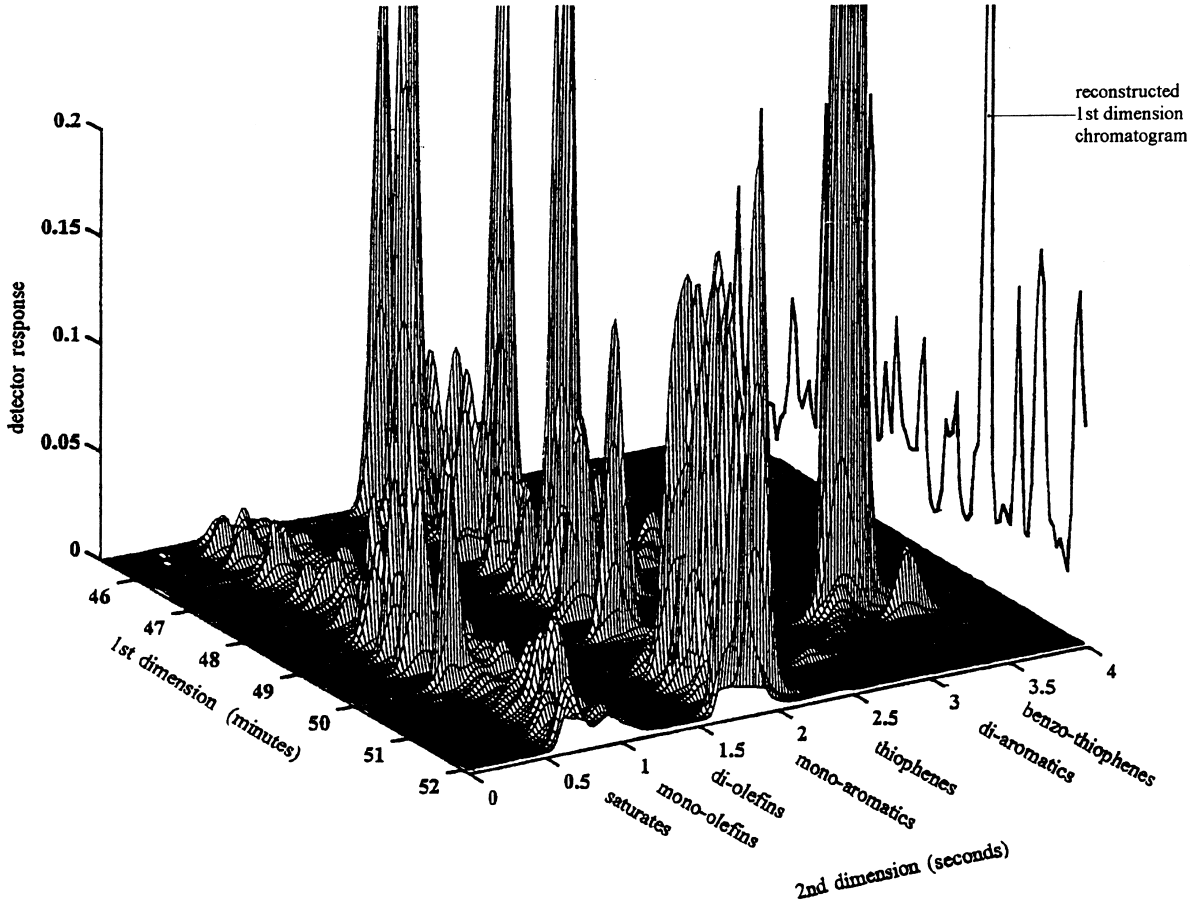

Fig. 1. 3D-plot of a (part of a) GC×GC separation of a heavy cat. cracked cycle oil.

pursued, viz. a group–type separation and a separation of target compounds. In a group–type separation, compounds of the same chemical class should be grouped together and separated from those of different classes. Separation within these classes is not always necessary. In GC×GC, compounds with comparable characteristics will have more or less identical second dimension retention times, and are therefore grouped together in bands along a 2D-plane. These characteristics can be molecular interactions, size or shape, depending on and determined by the two different stationary phases. The identification of compounds ordered within these bands is therefore greatly simplified by using reference compounds.

In the separation of target compounds, one strives to separate the compounds of interest from each other and from the matrix, either in the first and/or the second dimension. Compounds that are separated in the first column will always remain separated in the second column, since the two separation systems are chosen to be truly independent.

The 2D-separation in GC×GC is attained by combining two columns with different characteristics in series by means of a thermal modulator [5–7]. The operation of the thermal modulator (a short, narrow-bore capillary coated with a very thick film of stationary phase) used in this study and its effects are described elsewhere [8,9]. This thermal modulator interfaces the first and second dimension column. It accumulates, focuses and reinjects small fractions from the first column effluent with high speed at regular intervals onto the second column. The sample stream that elutes from the first dimension is chopped in a regular series of small fractions, focused and subsequently reinjected into a second and independent fast separation column. As stated, this column must be operated sufficiently fast for its separation to be finished before compounds from a next modulation will start to leave this second column. At each time a series of ''trains'' of separated compounds travels through the second column (see Fig. 2).

In order to get maximum separation performance in the GC×GC system, each individual first dimension peak should be modulated into several fractions (in general some five to ten). It can be calculated [5] that, for that purpose, the ratio of separation speeds between the second and first dimension separation must be at least of the order of 50.

To achieve this difference in speed, the second column may have a smaller internal diameter, a shorter length and/or a higher phase ratio ($\beta = r/2d_f$, where r is the column radius and d_f is the film thickness of the stationary phase). It is stressed that the ratio of separation speeds between the first and second column essentially determines whether GC× GC will work or not. A combination of, e.g., a ''wide-bore'' first column (0.53 mm I.D.) and a ''normal-bore'' second column (0.25 mm I.D.) will also produce the GC×GC effect.

The overall speed of the (total) GC×GC separation is determined by the maximum speed the second dimension separation allows and the speed and frequency of the modulation. In practice, the speed of modulation will be the limiting factor. This is caused by the fact that the transfer of heat from the sweeper, which performs the actual modulation, through the wall of the modulator capillary is limited. However, a newly designed sweeper can be used at frequencies up to 5 Hz [12].

Since the columns are coupled in series, the mass

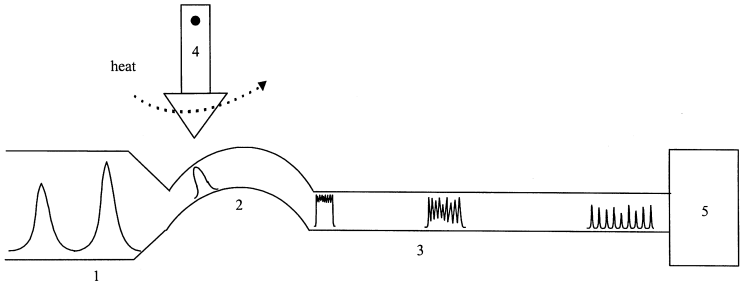

Fig. 2. Schematic diagram of the GC×GC separation system. (1) First dimension column; (2) modulator capillary; (3) second dimension column; (4) sweeper; (5) detector.

flow of the carrier gas through both columns is the same. Consequently, the average linear gas velocity in the two columns is quite different. And because both columns are located in one GC oven, both the carrier gas flow and the temperature influence the separation in the two dimensions simultaneously. It is therefore rather complicated to choose the appropriate columns and conditions needed to perform a specific separation. The construction of the two column set with the thermal modulator and determining the eventual GC×GC chromatogram is a rather labour-intensive task. A model able to simulate this chromatogram would be very helpful. Various authors have reported on calculation methods to predict retention times in linear temperature-programmed GC, even with serially coupled columns [10,11], but these models are unfit for use in GC×GC. These models assume that in serially coupled columns, components leaving the first column, subsequently are introduced into the second column for further separation. It is the aim of this study to develop a model to predict the eventual chromatogram from GC×GC for a given separation problem.

2. Theoretical

In order to predict the eventual chromatogram, we have to consider the parameters that determine the separations, and the way the two different separations are interrelated. The model we want to construct should preferably only need data that are generally and readily available, such as retention indices (k) and vapour pressure estimation methods.

2.1. Prediction of k

By Henry's law we may describe the partial pressure of a solute in dilute solutions as [13]:

$$p_i = x_{i,s}\gamma^{\infty}_{i,s}\, p_i^0 \tag{1}$$

where $x_{i,s}$ is the mole fraction of the solute in the stationary phase, $p_i{}^0$ is the vapour pressure of the pure solute and $\gamma^{\infty}_{i,s}$ is the activity coefficient (at infinite dilution) of the solute in the stationary phase. For the partition coefficient, i.e., the ratio of the concentrations of the solute in the mobile phase $c_{i,m}$ and in the stationary phase $c_{i,s}$ we find:

$$\frac{c_{i,s}}{c_{i,m}} = \frac{\rho_s RT}{M_s \gamma^{\infty}_{i,s} p_i^0} \tag{2}$$

where ρ_s and M_s are the density and the molecular mass of the stationary phase, R is the gas constant and T the temperature in degrees K. Since M_s/ρ_s represents the molar volume V_s of the stationary phase, the ratio of the amounts of solute in the stationary and the mobile phase becomes:

$$k = \frac{\rho_s RTV_s}{M_s \gamma^{\infty}_{i,s} p_i^0 V_m} = \frac{RTn_s}{\gamma^{\infty}_{i,s} p_i^0 V_m} \tag{3}$$

in which k is the retention factor, n_s is the total number of moles of the stationary phase and V_m the volume of the mobile phase.

From Eq. (3) we conclude that there are only two compound-dependent factors that affect retention. These are the vapour pressure of the pure solute, $p_i{}^0$, which is an exponential function of the temperature and the activity coefficient of the solute in the stationary phase, $\gamma^{\infty}_{i,s}$.

Regarding the vapour pressure, Antoine [14] proposed an equation for the estimation of that property, which has been widely used over limited temperature ranges:

$$\ln p_i^0 = A - \frac{B}{T + C} \tag{4}$$

Ref. [15] gives a table with the coefficients A, B and C for a number of compounds. For other compounds this table lists another set of the coefficients A, B, C and D, to be used in the Wagner [16] equation:

$$\ln p_i^0 = A - \frac{B}{T} + C \ln T + \frac{Dp_i^0}{T^2} \tag{5}$$

From these equations quite accurate vapour pressures of pure solutes in the chromatographic temperature range (300–600 K) can be calculated.

For a given column the total number of moles of stationary phase, n_s is constant. If we further assume for the moment that V_m is constant and independent on temperature and that $\gamma^{\infty}_{i,s}$ in Eq. (3) will be approximately constant for an homologous series, this equation can be rewritten into the simple form:

$$k = S(n_s, V_m, \gamma_i^{\infty})\frac{T}{p_i^0} \quad (6)$$

Here, $S(n_s, V_m, \gamma_i^{\infty})$ is a coefficient which depends on n_s, V_m and γ_i^{∞}. This implies that the experimental measurement of only one retention factor for a reference compound in an homologous series, yields an *S*-value that could be used for the whole series. Using this one experimental value at one temperature for *n*-nonane, we calculated *k* for the *n*-alkanes *n*-C_9 through *n*-C_{13} over the temperature range of 300–500 K using the Antoine Eq. (4) for the vapour pressures. After the Antoine Eq. (4) we would expect a linear relationship between log *k* and log *T*. We compare this equation with the measured values obtained on a 10 m capillary column coated with a 95% methyl–5% phenylpolysiloxane phase (DB-5 MS) (see Fig. 3). It is clear that the assumption that V_m and $\gamma_{i,s}^{\infty}$ in Eq. (3) are constants, is not completely true over the temperature range under consideration. The ratio's of the measured values of *k* and *T*, compared with the ratio's of the fitted values are significantly different. It appears that the deviation as expressed in the ratio's at $T=300$ and $T=470$ is about 20% in excess of the measured *k*-values. We examined which parameter in *S* is potentially responsible for this deviation in Fig. 3.

- The volume of the mobile phase, V_m, may change with temperature either by thermal expansion of the column, or from nonideality of the carrier gas (helium).
  - Calculation of the thermal expansion of the fused-silica column shows that the linear thermal expansion of the diameter of the column from 300 to 500 K is only approximately 0.1%.
  - The nonideality of the carrier gas, being helium, is expected to be very small as helium, is known as an almost ideal gas. Using generalised thermodynamic functions [15] we checked that the small virial coefficient of helium ($B(0)=0.0825$) does change only by 0.02% over the temperature range under consideration. Hence, at all temperatures helium can be considered as a truly ideal gas.
- So, only the change of γ_i^{∞} with temperature can be responsible for the difference between calculated and measured *k*-values. As explained else-

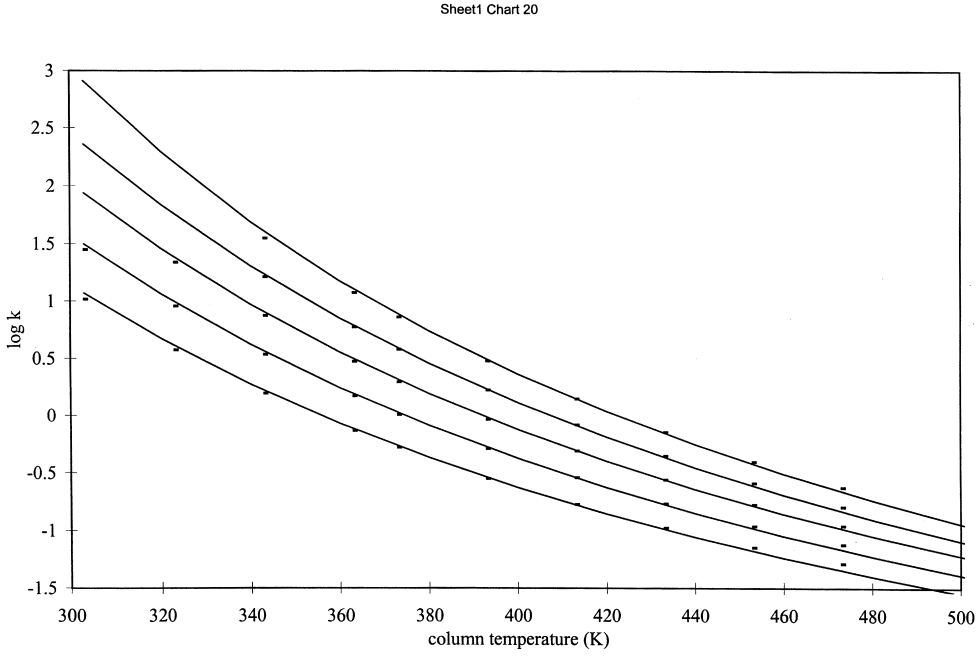

Fig. 3. Relationship between retention factor *k* and column temperature. The solid lines are fitted values, the dots represent the measured values (from bottom to top: *n*-C_9, *n*-C_{10}, *n*-C_{11}, *n*-C_{12} and *n*-C_{13}).

where [13,17,18] the activity coefficient can be regarded to consist of two independent parts, each one connected to the enthalpic and entropic parts of the partial molar excess free energy of mixing:

$$\ln \gamma_i = \ln \gamma_i^{\mathrm{h}} + \ln \gamma_i^{\mathrm{s}} \tag{7}$$

Here γ_i^{h} and γ_i^{s} are the enthalpic and entropic parts of the activity coefficient.

- The enthalpic or ''thermal'' contribution, which generally dominates, can be expressed as [13,17,18]:

$$\ln \gamma_{i,\mathrm{s}}^{\mathrm{h}} = \frac{\nu_i}{RT} \cdot (\partial_i - \partial_{\mathrm{s}})^2 \tag{8}$$

  in which v_i is the molar volume of the solute and δ_i and δ_{s} are the so-called ''solubility parameters'' of the solute and the stationary phase respectively. These parameters are defined as the square root of the cohesive energy density, i.e., the internal potential energy compared with the ideal gas state. As such they represent a measure for the affinity of solute and stationary phase molecules in their own environment. These parameters can be estimated with group increment models as proposed, e.g., by Fedors [19]. The change in γ_i^{∞} with temperature can thus be incorporated in the *S*-value when calculating *k* from Eq. (6), and this is found to be substantial.
- The ''athermal'' entropic contribution is found from the well-known Flory–Huggins expression [13,1,18,20,21]

$$\ln \gamma_i^{\mathrm{s}} = \ln \frac{v_i}{v_{\mathrm{s}}} + \left(1 - \frac{v_i}{v_{\mathrm{s}}}\right) \tag{9}$$

  Here v_i and v_{s} are the molar volumes of the solute and the stationary phase respectively. From this, the differences in the entropic contribution to γ_i^{∞} for the various *n*-alkanes can also be calculated and incorporated in *S* at all required temperatures.

2.1.1. Translation to GC×GC

The retention of a compound on the second dimension column in GC×GC is partly determined by the temperature of the column. Since both the first and the second dimension column are at the same temperature, the elution temperature (T_{E}) of a compound from the first column is also the (isothermal) temperature at which it is analysed on the second column. Once the elution temperature of the *n*-alkanes from the first column is known, we are able to estimate T_{E} for all the compounds we want to separate, from its Linear Programmed Temperature Retention Index (Linear Index) [22]

$$I^T = 100 \frac{t_{\mathrm{R}_i}^T - t_{\mathrm{R}_z}^T}{t_{\mathrm{R}_{(z+1)}}^T - t_{\mathrm{R}_z}^T} + 100z \tag{10}$$

Here $t_{\mathrm{R}}{}^T$ is the gross retention time, z and $z+1$ the number of C-atoms of the *n*-alkanes eluting before and after the compound *i* respectively. The Linear Indices are used for compounds eluting from temperature programmed columns. Its definition is such that it closely resembles that of the Kováts Retention Index used for isothermally operated columns [23].

$$I = 100 \frac{\log t'_{\mathrm{R}_i} - \log t'_{\mathrm{R}_z}}{\log t'_{\mathrm{R}_{(z+1)}} - \log t'_{\mathrm{R}_z}} + 100z \tag{11}$$

in which t'_{R} is the net retention time.

2.2. Prediction of the eventual chromatogram

From Eq. (6) and the corrections to *S* we are able to estimate *k* for the *n*-alkanes on the second column at the column temperature (=first dimension T_{E}) of the compounds we want to separate. From the carrier gas flow, the first column head pressure and the column dimensions, we can with the help of Poiseuille's law, calculate the second column head pressure. From this pressure and the second column dimensions we are able to calculate the second column dead time t_0. Using the increase in viscosity of the carrier gas with temperature [24], we are now able to calculate t_0 for each temperature. In between the virtual net retention times of the *n*-alkanes we may interpolate the net retention times of the compounds we want to separate. For that purpose we write Eq. (11) explicit in t'_{R_i}:

$$t'_{\mathrm{R}_i} = 10^{\log t_{\mathrm{R}_z}{}' \left(1 - \frac{I_i - I_z}{100}\right) + \log t_{\mathrm{R}_{(z+1)}}{}' \left(\frac{I_i - I_z}{100}\right)} \tag{12}$$

3. Experimental

3.1. Hardware

3.1.1. Gas chromatograph

Gas chromatograph: Hewlett Packard HP6890 (Wilmington, DE, USA), with the column bracket and modulator (prototype KT 2000 Retrofit kit; Zoex, Lincoln, NE, USA) for modulation and injection in the second dimension column as described elsewhere [8,9]. Injector: OPTIC 1 Programmed Temperature Vaporiser (PTV) (Ai, Cambridge, UK) in the split mode. The standard HP Flame Ionisation Detector (FID) is used for detection. The digital output signal was routed via the GC's RS-232 port to a RS-232 input board (National Instruments, Austin, TX, USA) of the PC, where it was further handled by the data acquisition software (see Section 3.2.1).

3.1.2. Columns

Three different sets of columns were used:

1. First dimension: 10 m×0.25 mm I.D., d_f=0.25 μm CP-Sil 2 CB (Chrompack, Middelburg, The Netherlands); modulation capillary: 0.07 m×0.10 mm I.D., d_f=3.0 μm SE-54 (Quadrex, New Haven, CT, USA); second dimension: 1.0 m×0.10 mm I.D., d_f=0.14 μm OV-1701 (Quadrex).
2. First dimension: 10 m×0.25 mm I.D., d_f=0.25 μm CP-Sil 2 CB (Chrompack); modulation capillary: 0.07 m×0.10 mm I.D., d_f=3.0 μm SE-54 (Quadrex); second dimension: 2.5 m×0.10 mm I.D., d_f=0.05 μm BPX50 (Scientific Glass Engineering, Ringwood, Australia).
3. First dimension: 10 m×0.25 mm I.D., d_f=0.25 μm DB-1 (J and W, Folsom, CA, USA); modulation capillary: 0.07 m×0.10 mm I.D., d_f=3.0 μm SE-54 (Quadrex); second dimension: 1.0 m×0.10 mm I.D., d_f=0.14 μm OV-1701 (Quadrex).

3.1.3. Operating conditions

The carrier gas used was helium, with a column head pressure of 100 kPa. The PTV was temperature programmed from 30°C at a rate of 16 C° s^{-1} to 400°C. The injected volume was 0.1 μl at a split ratio of 1:200. The GC oven was temperature programmed from 30°C at a rate of 2 C° min^{-1} to 225°C.

3.2. Software

3.2.1. Instrument control and data acquisition

The system was controlled by a PC with a GA 586AT mother board equipped with a 100 MHz Pentium processor and 132 MB DRAM. The control of the stepper motor for the sweeper movement and the data acquisition via the RS-232 port and input board was performed with software ''2D-GC'' rev. r.0.y (Southern Illinois University, Carbondale, IL, USA/Zoex), running under Labview rev. 3.1.1 (National Instruments). The speed of the sweeper in all experiments was 0.25 rev s^{-1} and the modulation time either 10 s or 4 s. For the representation of the 2D-chromatograms and contour plots we used SPYGLASS Transform rev. 3.0 (Spyglass. Champaign, IL, USA). Data processing of the data matrix file and integration of the peaks was performed by home made software ''Tweedee'', rev. 4.12 (University of Amsterdam, Amsterdam, The Netherlands) [9] running under MatLab rev. 4.2c.1 (MathWorks. Natick, MA, USA).

4. Results and discussion

4.1. Prediction of the GC×GC separation

4.1.1. Determining the column deadtime

In GC×GC, where the two columns are connected in series by means of the modulation capillary, it is impossible to measure the column deadtime t_0 of the second column directly. If we assume the total deadtime to be (within seconds) equal to the deadtime of the first column alone, there are a few means to determine t_0 indirectly.

1. For the second column, the vapour pressures of the *n*-alkanes can be calculated at different column temperatures with Eqs. (4) and (5). From these, second dimension retention factors can be

estimated with Eqs. (6), (8), (9). These retention factors will decrease with rising temperature and finally tend to approach $k=0$ as $p_i^0 \Rightarrow \infty$ and $t_0 \Rightarrow 0$. From a plot of retention factors vs. temperature (Fig. 3) t_0 can be estimated by extrapolation. This yields $t_0 = 0.5$ s, without correction for the *T*-dependency of the activity coefficient.

2. Similar curves could be obtained in practice after injecting a series of *n*-alkanes continuously onto the second dimension column. This situation was approached by injecting a series of *n*-alkanes by means of a nonheated PTV injector. The sample will then slowly evaporate and is more or less continuously fed to the column system. The first dimension column then produces enormous tails on each peak which will show up in the final 2D-plane as ''isovolatility'' lines. An example of seven *n*-alkanes is given in Fig. 4. Extrapolation of these lines yields the experimental t_0 at the point where all the lines fit into each other. The deadtime was estimated to be $t_0 = 0.44$ s.
3. An alternative method to measure t_0 has been investigated by doping the carrier gas with a small stream of 100 ppm methane in nitrogen. The FID will respond to methane with a stable response until the sweeper makes its turn. Two effects can be observed from the FID response in Fig. 5. When the sweeper starts heating the modulation capillary, it will locally increase the temperature of the carrier gas and thus the viscosity. This will instantly lead to less methane reaching the FID.

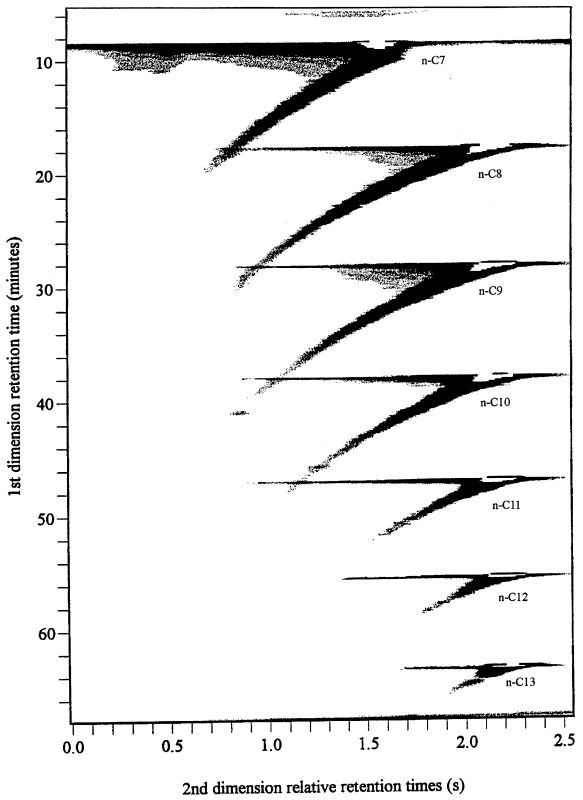

Fig. 4. ''Isovolatility'' lines of seven *n*-alkanes obtained from a GC×GC separation by continuous injection.

The start of the movement of the sweeper is thus indicated in the chromatogram by the decrease of the response. Since the modulator capillary is curved and the movement of the sweeper is curved into the opposite direction, the length over which the capillary is heated is different during the sweep time of 1.35 s. At the front end of the capillary it is heated over a length of 29 mm, in the middle over a length of 9 mm and at the end over a length of 23 mm. The flow disturbance, caused by increase of viscosity of the carrier is therefore different during the sweeper movement. The small amount of methane will be injected into the second column at the end of the sweep. This extra amount of methane will show up in the FID response. The difference of the end of the movement of the sweeper and the appearance of the extra peak yields $t_0 = 0.66$ s. It is seen that all three methods of estimating t_0 compare quite well.

4.1.2. Obtaining retention indices and elution temperatures

In order to predict the GC×GC separation of a specified sample, we need to know the Linear Indices of the compounds on the first and the Kováts Retention Indices on the second column. There are a number of retention index compilations available in literature, the Sadtler Library being the most extensive [25], but the more modern stationary phases are not included.

Generally speaking there is only a limited number of measured retention indices available on the modern (chemically bonded) phases. We therefore measured both the Kováts and the Linear Indices for a range of hydrocarbons on four different stationary phases. These data are collected in Tables 1–4.

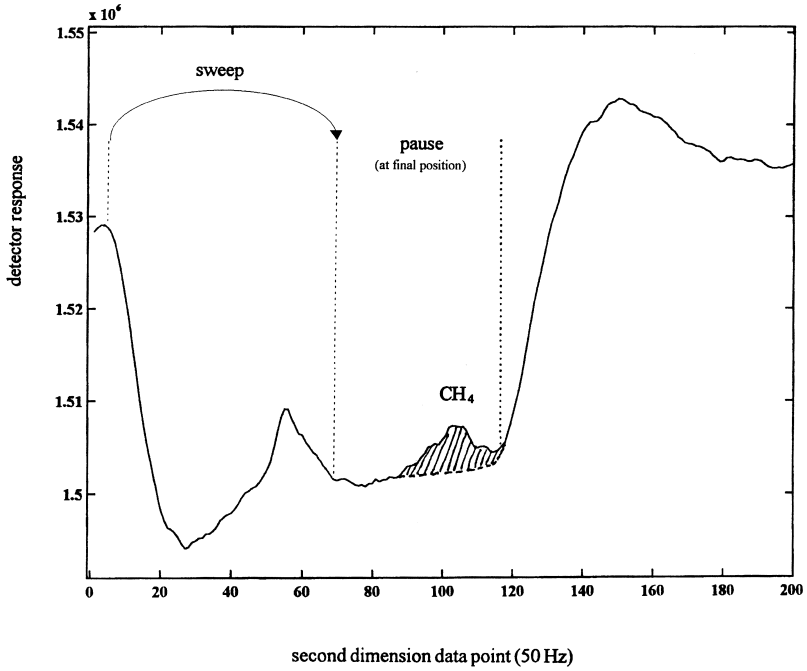

Fig. 5. Second dimension chromatogram of the methane supply method. The different minima in the response between sample point ≠25 and ≠80 are caused by heating the (curved) modulator capillary over distances of 29 mm, 9 mm and 23 mm respectively.

In addition to these retention indices, the T_E values of the compounds on the first column have to be known. For hydrocarbons it is sufficient to measure the retention times of a few *n*-alkanes covering the boiling point range of interest, on a column similar to the one intended to be used as the first column. For nonhydrocarbons, these values can be calculated from their retention indices and the indices and T_E values of the *n*-alkanes, or have to be measured. Using the flow and temperature program intended to be used in GC×GC, the resulting retention times can be used directly. Experiments showed that upon adding a second dimension column (which has a rather high pressure drop), retention times remained virtually constant, and so their T_E values also remained virtually constant. Since the retention times on a linear temperature programmed column and the boiling points of *n*-alkanes (above *n*-dodecane) follow a strictly linear relationship, the retention times may be interpolated from the boiling points of the interjacent *n*-alkanes. From these retention times, the Linear Indices and the temperature program we are able to calculate elution temperatures of all the individual compounds of interest on the first column.

4.1.3. Calculating the eventual GC×GC chromatogram

4.1.3.1. The predicted retention times

The calculated T_E-values of the compounds from the first column are also the temperatures at which these compounds will be analysed on the second column. From the calculated vapour pressures of the *n*-alkanes at these temperatures (Eq. (4) or Eq. (5)) we find the retention factor *k* of these *n*-alkanes with the help of Eq. (6), taking Eqs. (7) and (8) into account. Thereto we used for the value of *S* in Eq. (6) for our reference compound *n*-nonane, eluting around 330 K, the experimental value of 0.0004 as found earlier on short (1–2 metres), thin film, microbore columns. With known t_0 of the second column, we now calculate the virtual net retention times of the *n*-alkanes. Logarithmic interpolation according to Eq. (12) gives the retention times of the compounds of interest. Combining the retentions on

Table 1
Retention indices: measured with 8 m×0.25 mm I.D., 0.25 μm DB-1 (DB-1, J and W) in HP 6890 with Optic PTV injector (Ai) @150°C+12 C° s^{-1}⇒300°C; carrier helium, 40 kPa, 0.7 ml min^{-1}

eCompound	Boiling point (°C)	Kováts Index (@60°C)	Kováts Index (@140°C)	Linear Index (30°C+2 C° min^{-1})
Benzene	80.1	–	668	639
n-Heptane	98.4	700	700	700
Methyl-cyclohexane	100.9	726	754	715
Toluene	110.6	754	767	742
1-Octene	121.3	788	789	785
n-Octane	125.7	800	800	800
Ethyl-cyclohexane	131.8	829	851	818
Ethylbenzene	136.2	847	861	834
1-Nonene	146.9	889	889	884
n-Nonane	150.8	900	900	900
n-Propyl-cyclohexane	156.7	926	951	916
n-Propylbenzene	159.2	940	961	928
1-Decene	170.6	990	989	985
n-Decane	174.1	1000	1000	1000
n-Butyl-cyclohexane	180	1024	1047	1018
n-Butylbenzene	183.3	1039	1058	1030
1-Undecene	192.7	1090	1087	1086
n-Undecane	195.9	1100	1100	1100
n-Pentyl-cyclohexane	202	1122	1147	1121
1-Dodecene	213.4	1189	1188	1187
n-Dodecane	216.3	1200	1200	1200
n-Hexyl-cyclohexane	222	1222	1246	1224
n-Hexylbenzene	226.1	1239	1255	1233
1-Tridecene	232.8	1289	1288	1287
n-Tridecane	235.4	1300	1300	1300
n-Heptyl-cyclohexane	241	1322	1346	1328
n-Heptylbenzene	246.1	1338	1355	1337
1-Tetradecene	251.1	1388	1388	1388
n-Tetradecane	253.5	1400	1400	1400
n-Octyl-cyclohexane	259	–	1447	1432
n-Octylbenzene	264.4	–	1456	1439
1-Pentadecene	268.4	–	1488	1487
n-Pentadecane	270.6	1500	1500	1500
n-Nonyl-cyclohexane	276	–	1546	1536
1-Hexadecene	284.9	–	1588	1587
n-Hexadecane	286.8	1600	1600	1600
n-Decylbenzene	297.9	–	1655	1645
1-Heptadecene	300.3	–	1689	1687
n-Heptadecane	302.2	1700	1700	1700
1-Octadecene	314.8	–	1793	1788
n-Octadecane	316.7	1800	1800	1800

the first and second column will finally produce the coordinates of the peaks in the chromatogram.

4.1.3.2. The predicted peak widths

Assuming negligible extracolumn contribution to band broadening from detector volume and electronics, the final peak widths of the peaks on the second column can be estimated by applying the rule of additivity of variances [26]:

$$\sigma_t^2 = \sigma_i^2 + \sigma_c^2 \quad (13)$$

in which σ_t is the final band width in terms of standard deviations, σ_i the input band width and σ_c

Table 2
Retention indices: measured with 10 m×0.25 mm I.D., 0.25 μm CP-Sil 2 CB (Chrompack) in HP 6890 with Optic PTV injector (Ai) @150°C+12 C° s^{-1}⇒300°C; carrier helium, 200 kPa, 0.7 ml min^{-1}

Compound	Boiling point (°C)	Kováts Index (@60°C)	Kováts Index (@140°C)	Linear Index (30°C+2 C° min^{-1})
Benzene	80.1	649	678	693
n-Heptane	98.4	700	700	700
Methyl-cyclohexane	100.9	733	772	730
Toluene	110.6	758	752	752
1-Octene	121.3	783	783	782
n-Octane	125.7	800	800	800
Ethyl-cyclohexane	131.8	843	865	830
Ethylbenzene	136.2	848	873	836
1-Nonene	146.9	883	884	882
n-Nonane	150.8	900	900	900
n-Propyl-cyclohexane	156.7	936	962	928
n-Propylbenzene	159.2	937	965	930
1-Decene	170.6	984	986	983
n-Decane	174.1	1000	1000	1000
n-Butyl-cyclohexane	180	1034	1061	1029
n-Butylbenzene	183.3	1036	1065	1033
1-Undecene	192.7	1083	1086	1084
n-Undecane	195.9	1100	1100	1100
n-Pentyl-cyclohexane	202	1132	1160	1133
1-Dodecene	213.4	1183	1186	1185
n-Dodecane	216.3	1200	1200	1200
n-Hexyl-cyclohexane	222	1231	1259	1237
n-Hexylbenzene	226.1	1234	1260	1237
1-Tridecene	232.8	1284	1286	1285
n-Tridecane	235.4	1300	1300	1300
n-Heptyl-cyclohexane	241	–	1359	1342
n-Heptylbenzene	246.1	–	1360	1343
1-Tetradecene	251.1	–	1386	1386
n-Tetradecane	253.5	1400	1400	1400
n-Octyl-cyclohexane	259	–	1460	1448
n-Octylbenzene	264.4	–	1459	1447
1-Pentadecene	268.4	–	1486	1488
n-Pentadecane	270.6	1500	1500	1500
n-Nonyl-cyclohexane	276	–	1560	1552
1-Hexadecene	284.9	–	1586	1586
n-Hexadecane	286.8	1600	1600	1600
n-Decylbenzene	297.9	–	1659	1653
1-Heptadecene	300.3	–	1686	–
n-Heptadecane	302.2	1700	1700	1700
1-Octadecene	314.8	–	1786	–
n-Octadecane	316.7	1800	1800	1800

the chromatographic band broadening. The input band width is caused by the thermal modulation and the interface between the modulator capillary and the second column. It was measured to be $\sigma_i = 0.07$ s, which is considered a typical value for this version of the thermal modulator under the present temperature, flow-rate and modulator capillary length [12].

The chromatographic band broadening can be calculated from:

$$\sigma_c^2 = \frac{t_{R_i}^2}{N} \tag{14}$$

in which t_{R_i} is the retention time and N the number

Table 3
Retention indices: measured with 10 m×0.10 mm I.D., 0.21 μm CP-Sil 19 CB (Chrompack), a substitute for OV-1701 in HP 6890 with Optic PTV injector (Ai) @150°C+12 C° s^{-1}⇒300°C; carrier helium, 400 kPa, 0.7 ml min^{-1}

Compound	Boiling point (°C)	Kováts Index (@60°C)	Kováts Index (@140°C)	Linear Index (30°C+2 C° min^{-1})
Benzene	80.1	718	750	720
n-Heptane	98.4	700	700	700
Methyl-cyclohexane	100.9	732	788	734
Toluene	110.6	821	853	811
1-Octene	121.3	802	805	801
n-Octane	125.7	800	800	800
Ethyl-cyclohexane	131.8	837	869	828
Ethylbenzene	136.2	914	944	906
1-Nonene	146.9	902	904	901
n-Nonane	150.8	900	900	900
n-Propyl-cyclohexane	156.7	939	968	930
n-Propylbenzene	159.2	1003	1033	1001
1-Decene	170.6	1002	1005	1002
n-Decane	174.1	1000	1000	1000
n-Butyl-cyclohexane	180	1038	1066	1031
n-Butylbenzene	183.3	1103	1132	1103
1-Undecene	192.7	1103	1104	1102
n-Undecane	195.9	1100	1100	1100
n-Pentyl-cyclohexane	202	1132	1165	1135
1-Dodecene	213.4	1202	1203	1202
n-Dodecane	216.3	1200	1200	1200
n-Hexyl-cyclohexane	222	1237	1265	1239
n-Hexylbenzene	226.1	1298	1328	1303
1-Tridecene	232.8	1302	1303	1302
n-Tridecane	235.4	1300	1300	1300
n-Heptyl-cyclohexane	241	–	1365	1344
n-Heptylbenzene	246.1	1399	1429	1410
1-Tetradecene	251.1	1402	1404	1404
n-Tetradecane	253.5	1400	1400	1400
n-Octyl-cyclohexane	259	–	1466	1450
n-Octylbenzene	264.4	–	1528	1512
1-Pentadecene	268.4	–	1503	1503
n-Pentadecane	270.6	1500	1500	1500
n-Nonyl-cyclohexane	276	–	1565	1556
1-Hexadecene	284.9	–	1603	1602
n-Hexadecane	286.8	1600	1600	1600
n-Decylbenzene	297.9	–	1721	1720
1-Heptadecene	300.3	–	1703	1703
n-Heptadecane	302.2	1700	1700	1700
1-Octadecene	314.8	–	1802	1802
n-Octadecane	316.7	1800	1800	1800

of theoretical plates of the second column. The final peak widths of the compounds (being $4\sigma_t$) can now be estimated.

In Fig. 6 a block diagram is presented in which all the individual steps for the prediction of the eventual chromatogram are indicated.

In Fig. 7a we present a predicted chromatogram of the separation of twelve hydrocarbon compounds; for comparison the chromatogram of the experimental GC×GC separation is presented as a contour plot in Fig. 7b. Column set 1 was used for this separation.

A second example is given in Fig. 8a and b for the same compounds, separated with column set 2. For a different mixture of eleven hydrocarbons, the pre-

Table 4
Retention indices: measured with 12 m×0.10 mm I.D., 0.05 μm BPX50 (SGE) in HP 6890 with Optic PTV injector (Ai) @150°C+12 C° s^{-1}⇒300°C; carrier helium, 400 kPa, 0.7 ml min^{-1}

Compound	Boiling point (°C)	Kováts Index (@60°C)	Kováts Index (@140°C)	Linear Index (60°C+2 C° min^{-1})
Benzene	80.1	778	810	770
n-Heptane	98.4	700	700	700
Methyl-cyclohexane	100.9	713	739	797
Toluene	110.6	876	907	871
1-Octene	121.3	807	810	808
n-Octane	125.7	800	800	800
Ethyl-cyclohexane	131.8	841	863	873
Ethylbenzene	136.2	970	1000	966
1-Nonene	146.9	910	913	911
n-Nonane	150.8	900	900	900
n-Propyl-cyclohexane	156.7	962	1000	961
n-Propylbenzene	159.2	1056	1092	1052
1-Decene	170.6	1011	1012	1007
n-Decane	174.1	1000	1000	1000
n-Butyl-cyclohexane	180	1061	1100	1054
n-Butylbenzene	183.3	1154	1192	1153
1-Undecene	192.7	1111	1113	1108
n-Undecane	195.9	1100	1100	1100
n-Pentyl-cyclohexane	202	1160	1200	1155
1-Dodecene	213.4	1211	1214	1208
n-Dodecane	216.3	1200	1200	1200
n-Hexyl-cyclohexane	222	1260	1298	1259
n-Hexylbenzene	226.1	1353	1389	1355
1-Tridecene	232.8	1310	1313	1308
n-Tridecane	235.4	1300	1300	1300
n-Heptyl-cyclohexane	241	1362	1396	1365
n-Heptylbenzene	246.1	1454	1489	1458
1-Tetradecene	251.1	1414	1414	1409
n-Tetradecane	253.5	1400	1400	1400
n-Octyl-cyclohexane	259	1467	1497	1469
n-Octylbenzene	264.4	–	1588	1565
1-Pentadecene	268.4	–	1514	1508
n-Pentadecane	270.6	1500	1500	1500
n-Nonyl-cyclohexane	276	–	1596	1572
1-Hexadecene	284.9	–	1612	1608
n-Hexadecane	286.8	1600	1600	1600
n-Decylbenzene	297.9	–	1789	1771
1-Heptadecene	300.3	–	1711	1707
n-Heptadecane	302.2	1700	1700	1700
1-Octadecene	314.8	–	1812	1808
n-Octadecane	316.7	1800	1800	1800

dicted and experimental chromatogram, using column set 3, are presented in Fig. 9a and b.

From all these examples it is clear that the model to predict the eventual chromatogram is rather accurate and can be used to judge whether a certain column combination is suited to produce a desired separation.

4.2. Tuning of the GC×GC separation

Although the chromatogram can be predicted quite nicely, each set of columns must be tuned by varying the column length, the phase ratio and the flow. All these variables affect the elution temperature as is depicted schematically in Fig. 10. By choosing a

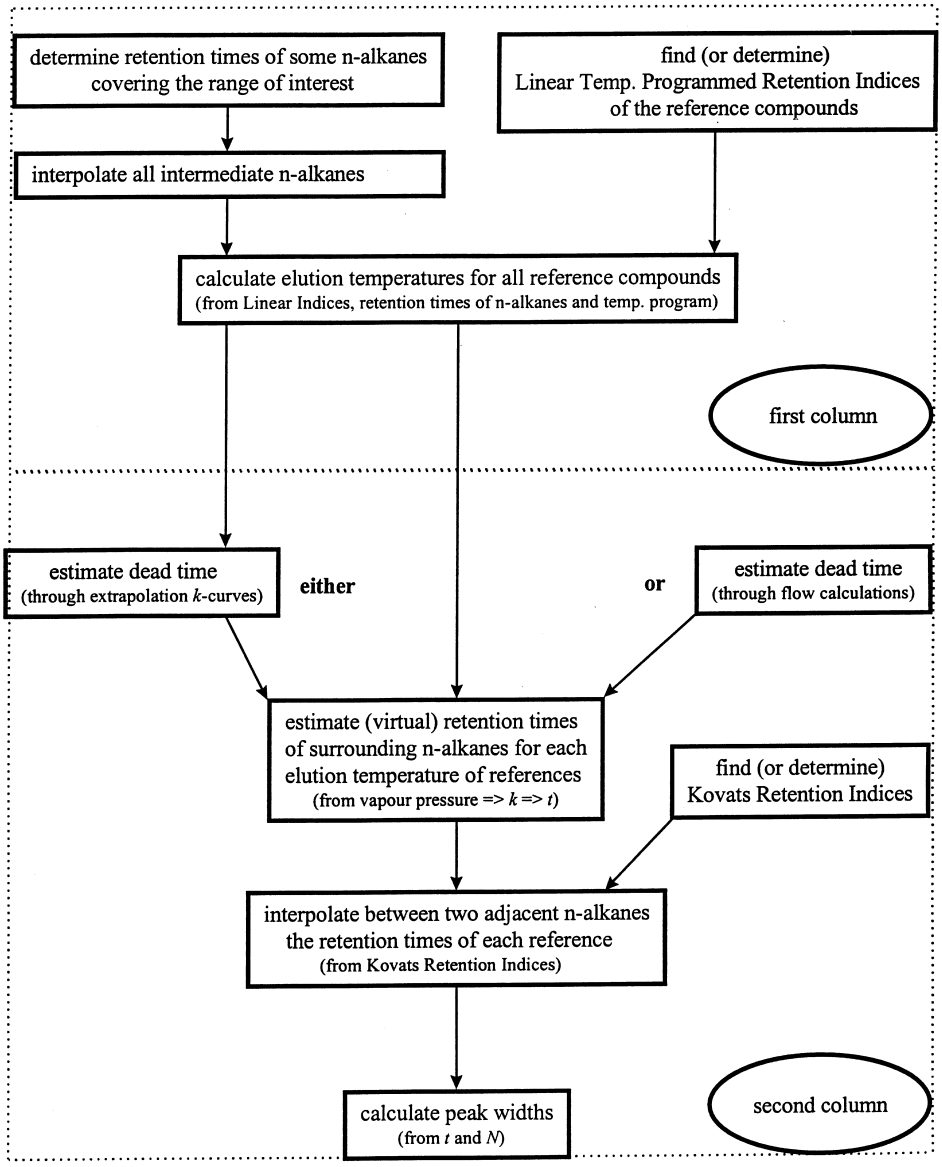

Fig. 6. Block diagram of the calculation steps to predict a GC×GC chromatogram.

lower phase ratio of the first column, T_E will increase and hence the k-values on the second column will decrease. By decreasing the flow-rate, T_E of the first column will increase slightly, but the retention factors on the second column will decrease. Once these parameters are set satisfactory, the frequency, speed and temperature of the thermal modulator can be set.

5. Conclusion

With the help of the developed and tested model, we are able to accurately predict a GC×GC chromatogram. The data required, are vapour pressures and Linear Temperature Programmed Indices measured on a column at conditions similar to those used in the GC×GC combination. Furthermore Kováts

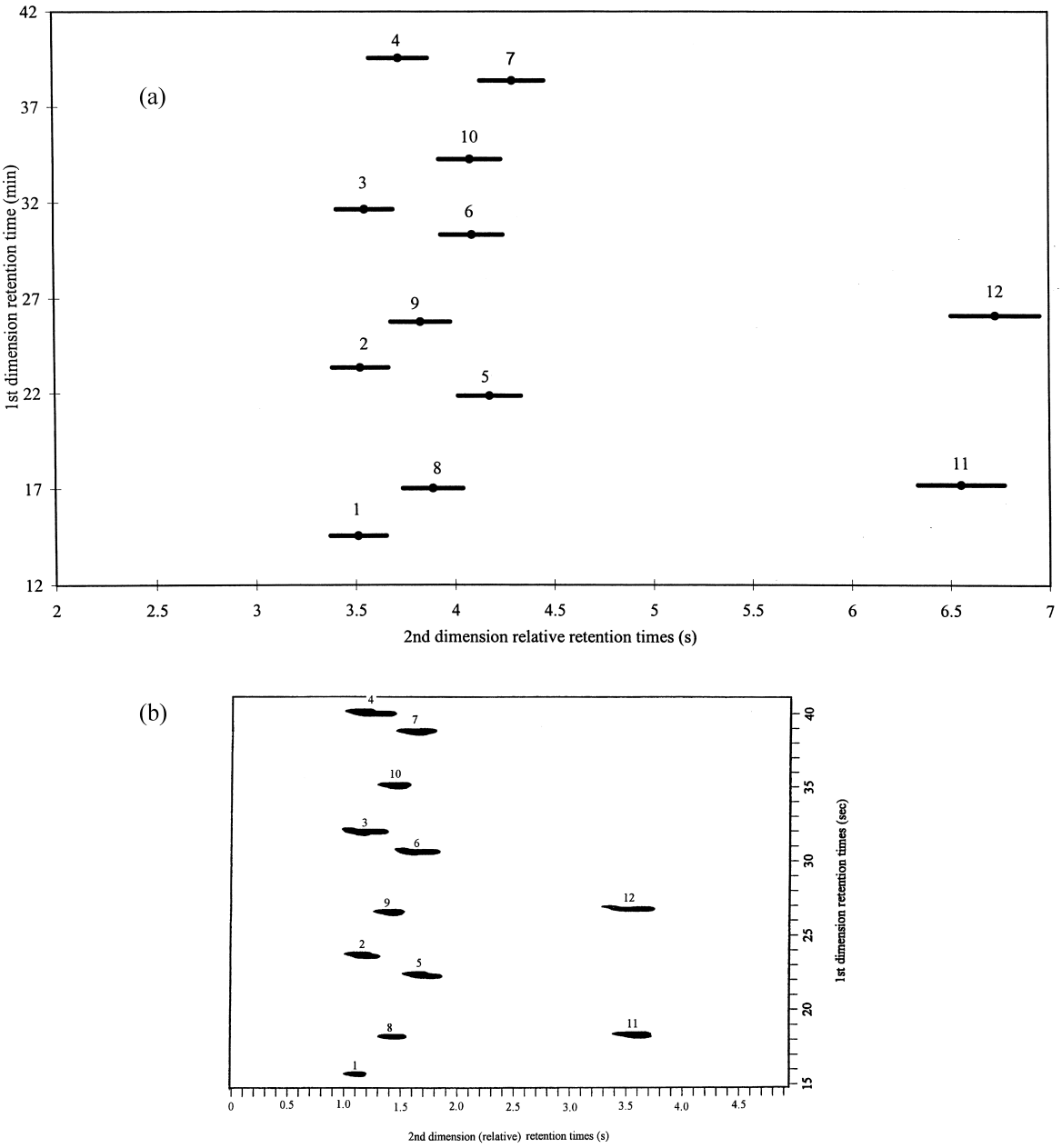

Fig. 7. (a) Predicted GC×GC chromatogram of twelve compounds with column set 1. (1) *n*-C_9; (2) *n*-C_{10}; (3) *n*-C_{11}; (4) *n*-C_{12}; (5) 1-C_{10}=; (6) 1-C_{11}=; (7) 1-C_{12}=; (8) *n*-prop-cyclo C_6; (9) *n*-but-cyclo C_6; (10) *n*-pent-cyclo C_6; (11) *n*-prop-benzene; (12) *n*-but-benzene. (b) Experimental chromatogram of the same compounds with column set 1.

Retention Indices of all the compounds we want to predict, measured on the stationary phase of the second column, are needed for extrapolation purposes and as a measure for the activity coefficients. With these data available, the predicted chromatogram is very much comparable with the experimental chromatogram. A limitation to the freedom of choice of the combination of the two different columns is

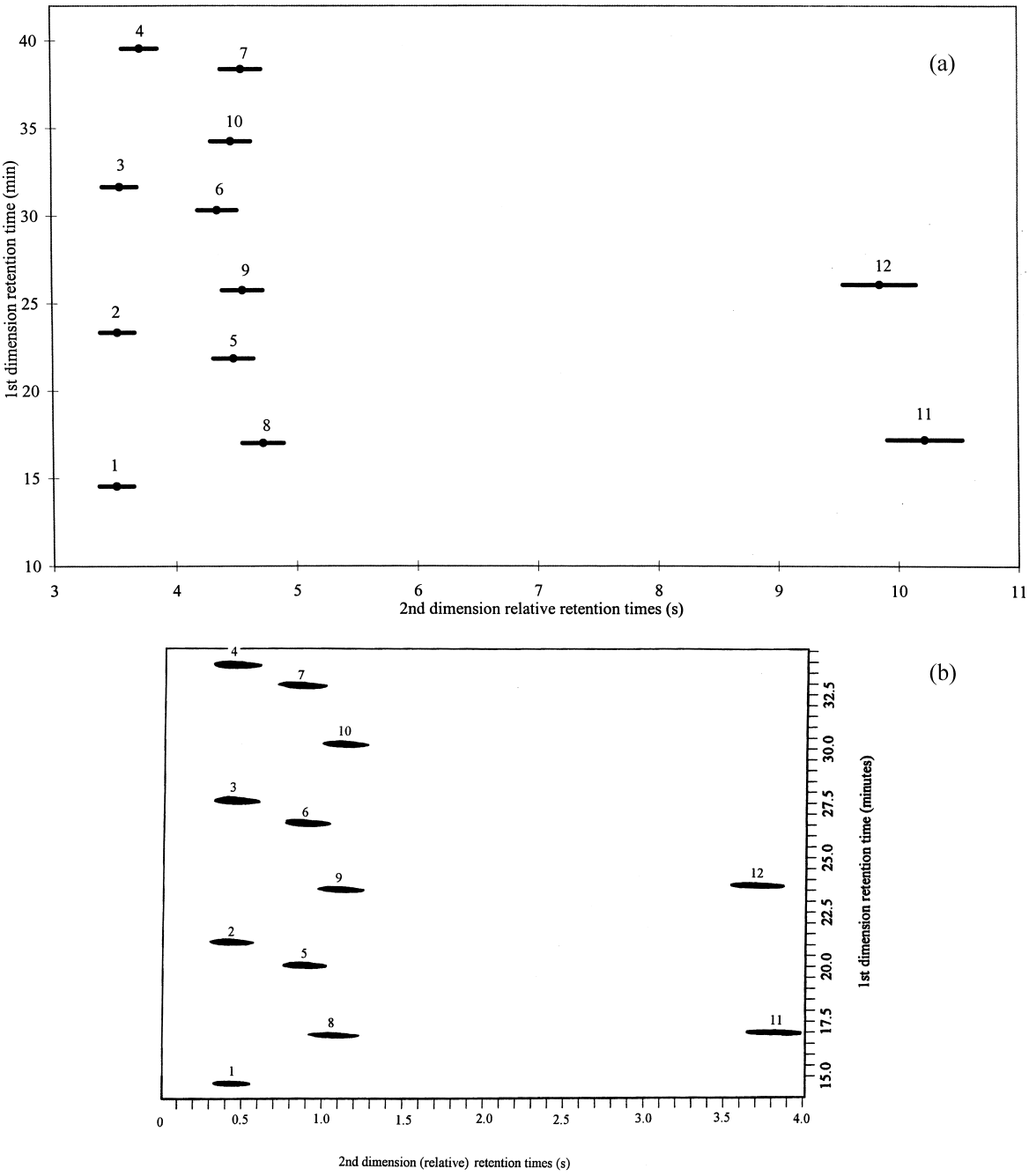

Fig. 8. (a) Predicted GC×GC chromatogram of twelve compounds with column set 2. Compounds the same as in Fig. 7a and b. (b) Experimental chromatogram of the same compounds with column set 2.

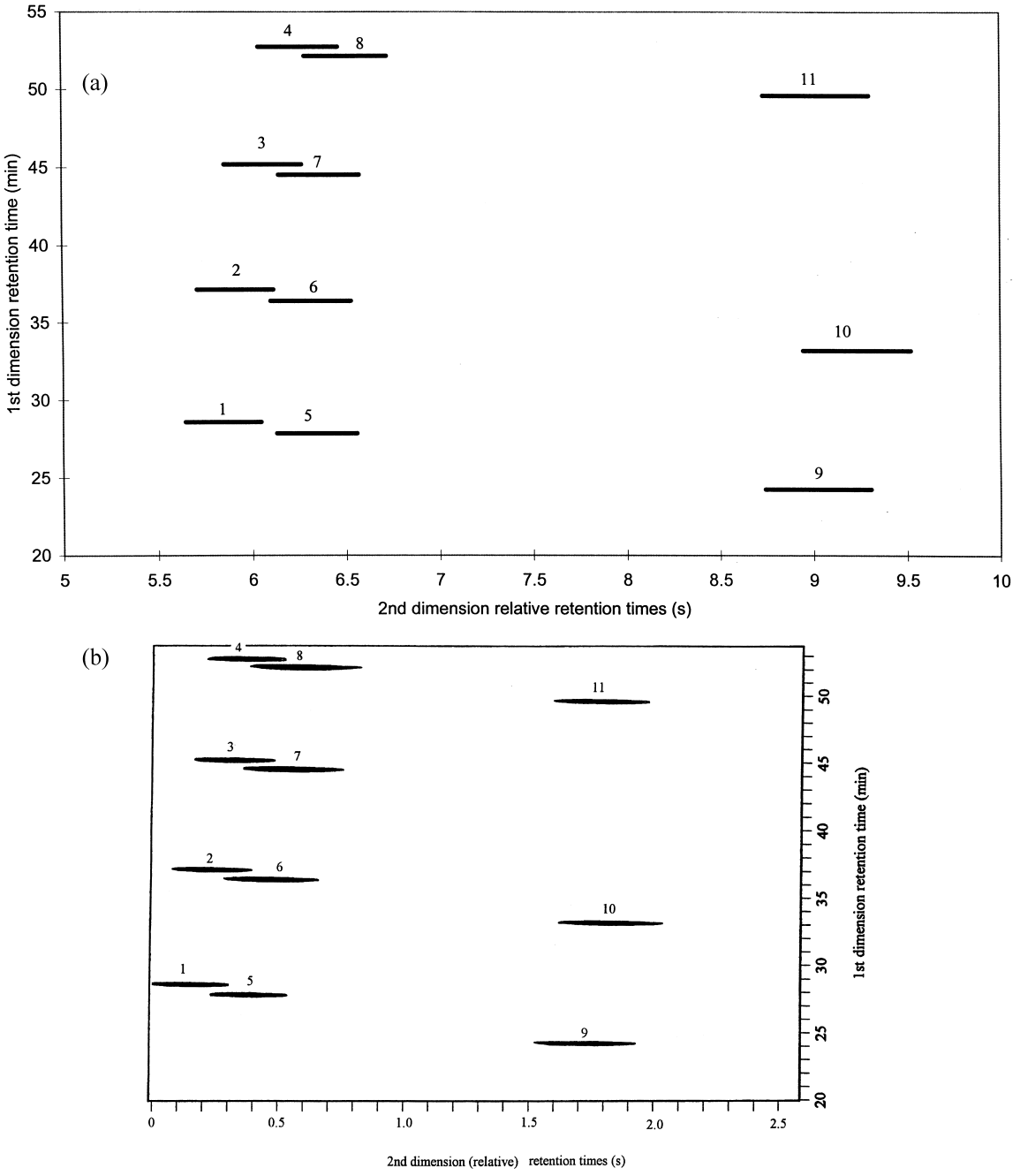

Fig. 9. (a) Predicted GC×GC chromatogram of eleven compounds with column set 3. (1) *n*-C_{10}; (2) *n*-C_{11}; (3) *n*-C_{12}; (4) *n*-C_{13}; (5) 1-C_{10}=; (6) 1-C_{11}=; (7) 1-C_{12}=; (8) 1-C_{13}=; (9) *n*-prop-benzene; (10) *n*-but-benzene; (11) *n*-hex-benzene. (b) Experimental chromatogram of the same compounds with column set 3.

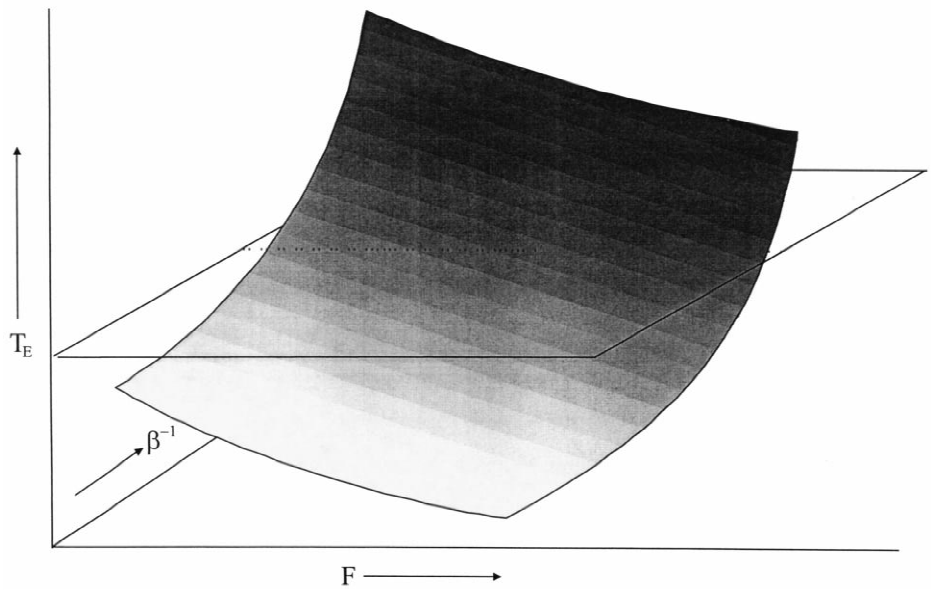

Fig. 10. Relationship between elution temperature, phase ratio and carrier gas flow.

the fact that both columns cannot (yet) be temperature programmed independently.

Acknowledgements

The fruitful discussions with Peter Schoenmakers of Shell Research and Technology Centre, Amsterdam and with Hans-Gerd Janssen of Eindhoven University of Technology were very much appreciated.

References

[1] W. Bertsch, Recent advances in capillary gas chromatography, Chromatogr. Methods, 1981, Ch. 1, pp. 3–55.
[2] W. Bertsch, Multdimensional GC, in: H.J. Cortes, (Ed.), Multidimensional Chromatography, Chromatographic Science Series, Vol. 50, Marcel Dekker, New York, 1990, Ch. 3, pp. 74–144.
[3] G.W. Kelly, K.D. Bartle, J. High Resolut. Chromatogr. 17 (1994) 390.
[4] K. Grob, Proceedings of the 16th Int. Symp. on Capillary Chromatography, Riva del Garda, Hüthig Verlag, Heidelberg, 1994.
[5] Z. Liu, J.B. Phillips, J. Chromatogr. Sci. 29 (1991) 227.
[6] C.J. Venkatramani, J.B. Phillips, J. Microcol. Sep. 5 (1993) 511.
[7] J.B. Phillips, J. Xu, J. Chromatogr. A 703 (1995) 327.
[8] J. Blomberg, P.J. Schoenmakers, J. Beens, R. Tijssen, J. High Resolut. Chromatogr. 20 (1997) 539.
[9] J. Beens, R. Tijssen, J. Blomberg, P.J. Schoenmakers, J. High Resolut. Chromatogr. 21 (1998) 47.
[10] L.H. Wright, J.F. Walling, J. Chromatgr. 540 (1991) 311.
[11] T.C. Gerbino, G. Castello, J. High Resolut. Chromatogr. 17 (1994) 597.
[12] J.B. Phillips, R.B. Gaines, J. Blomberg, P.J. Schoenmakers, F.W.M. van der Wielen, J. Dimandja, V. Green, J. Granger, D. Patterson, L. Racovalis, H-J. de Geus, J. de Boer, P. Haglund, J. Lipsky, E.B. Ledford, J. High Resolut. Chromatogr. accepted.
[13] P.J. Schoenmakers, Optimization of Chromatographic Selectivity, Journal of Chromatography Library, Elsevier, Amsterdam, vol. 35, 1986, pp. 37 and 38.
[14] C. Antoine, C.R. 107 (1888) 681.
[15] R.C. Reid, J.M. Prausnitz, B.E. Poling, The Properties of Gases and Liquids, fourth ed., McGraw–Hill, New York, 1987, pp. 656–732.
[16] W. Wagner, Cryogenics 13 (1973) 470.
[17] R. Tijssen, H.A.H. Billiet, P.J. Schoenmakers, J. Chromatogr. 122 (1976) 185.
[18] R. Tijssen, P.J. Schoenmakers, M.R. Böhmer, L.K. Koopal, H.A. Billiet, J. Chromatogr. A 656 (1993) 135.
[19] R.F. Fedors, Polym. Eng. Sci. 14(2) (1974) 147.
[20] B.L. Karger, L.R. Snyder, Cs. Horvath, An Introduction to Separation Science, Wiley, New York, 1973.

[21] D.H. Everett, R.J. Munn, Trans. Faraday Soc. 60 (1964) 1951.
[22] H. van den Dool, P.D. Kratz, J Chromatogr. 11 (1963) 463.
[23] Sz.E. Kováts, Helv. Chim. Acta 41 (1958) 1915.
[24] J.V. Hinshaw, L.S. Ettre, J. High Resolut. Chromatogr. 20 (1997) 472.
[25] The Sadtler Standard Gas Chromatography Retention Index Library, Sadtler Research Laboratories, Philadelphia, 1985.
[26] A. van Es, High Speed Narrow Bore Capillary Gas Chromatography, Chromatographic Methods, Hüthig Verlag, Heidelberg, 1992.